arXiv:hep-ph/9603290v2 20 Mar 1996

Dilepton and Photon Emission Rates from a Hadronic Gas

James V. Steele[1], **Hidenaga Yamagishi**[2] and **Ismail Zahed**[1]
[1]*Department of Physics, SUNY, Stony Brook, New York 11794, USA;*
[2]*4 Chome 11-16-502, Shimomeguro, Meguro, Tokyo, Japan. 153.*

(February 1, 2008)

We analyze the dilepton and photon emission rates from a hadronic gas using chiral reduction formulas and a virial expansion. The emission rates are reduced to pertinent vacuum correlation functions, most of which can be assessed from experiment. Our results indicate that in the low mass region, the dilepton and photon rates are enhanced compared to most of the calculations using chiral Lagrangians. The enhancement is further increased through a finite pion chemical potential. An estimate of the emission rates is also made using Haag's expansion for the electromagnetic current. The relevance of these results to dilepton and photon emission rates in heavy-ion collisions is discussed.

1. Recent fixed target experiments at the CERN SPS using ultra-relativistic heavy-ion collisions have reported an excess of dielectrons (CERES) [1] and dimuons (HELIOS3) [2] over a broad range of dilepton invariant mass starting from the two-pion threshold. Some enhancement in the photon emission rate has been reported by WA80 [3] although the direct photon measurements by CERES and HELIOS3 seem to suggest that the excess is within statistical errors when the Dalitz decays are subtracted out. The latter constitute 90% of the photon spectrum below the two-pion threshold.

Enhancements in either the dilepton or photon spectra do not seem to follow from calculations using chiral Lagrangians in hadronic phase [4,5] or high temperature QCD for the quark-gluon phase [6], although neither of them is assumption free for temperatures around the pion mass. A rate departure from p-A collisions may be indicative of some medium modifications [7] in the hadronic phase, although the rate may be enhanced or depleted [8] depending on model assumptions.

In view of this, it is important that the rate calculations are reassessed in as model independent way as possible. Also, since the dilepton and photon emission rates originate from the same current-current correlation *albeit* with different kinematics, it is important that both rates are assessed simultaneously in a consistent manner. Better photon and dilepton measurements are yet to come, putting to test our understanding of the strong interactions in the hot hadronic phase.

In this letter we will show that in a thermal hadronic environment with a temperature near or below the pion mass the dilepton and photon emission rates are directly related to the absorptive parts of the scattering amplitudes of virtual and real photons off an arbitrary number of on-shell pions. These scattering amplitudes are reducible to pertinent vacuum correlation functions using chiral reduction formulas [9]. To leading order in the pion density, the emission rates are constrained by data from electro-production and -annihilation, tau-decays, pion radiative decay and two-photon fusion reactions. Our results indicate that in the low mass region the dilepton and photon rates are enhanced in comparison with calculations using explicit reaction processes from chiral Lagrangians. There is also an enhancement for finite pion chemical potential in both cases. For comparison, we also give a direct estimate for the emission rates using Haag's expansion for the electromagnetic current. The relevance of our results to lepton and photon emission from heavy-ion collisions is discussed.

2. In a hadronic gas in thermal equilibrium, the rate $\mathbf{R}$ of dileptons produced in a unit four volume follows from the thermal expectation value of the electromagnetic current-current correlation function [10]. For massless leptons with momenta p_1, p_2, the rate per unit dilepton momentum $q = p_1 + p_2$ is given by

$$\frac{d\mathbf{R}}{d^4q} = -\frac{\alpha^2}{6\pi^3 q^2}\ \ \mathbf{W}(q) \tag{1}$$

where $\alpha = e^2/4\pi$ is the fine structure constant,

$$\mathbf{W}(q) = \int d^4x\, e^{-iq\cdot x}\, \mathrm{Tr}\left(e^{-(\mathbf{H}-F)/T}\ \mathbf{J}^\mu(x)\mathbf{J}_\mu(0)\right), \tag{2}$$

$e\mathbf{J}_\mu$ is the hadronic part of the electromagnetic current, $\mathbf{H}$ is the hadronic Hamiltonian, F the free energy, T the temperature, and the trace is over a complete set of hadron states. We have set the pion chemical potential to zero. The results for a non-zero pion chemical potential are discussed in section 5. For leptons with mass m_l, the right-hand side of (1) is multiplied by

$$(1+\frac{2m_l^2}{q^2})(1-\frac{4m_l^2}{q^2})^{\frac{1}{2}}. \tag{3}$$

From the spectral representation and symmetry, the rate may also be expressed in terms of the absorptive part of the time-ordered function

$$\mathbf{W}(q) = \frac{2}{1+e^{q^0/T}}\ \mathrm{Im}\mathbf{W}^F(q) \tag{4}$$

$$\mathbf{W}^F(q) = i\int d^4x\, e^{iq\cdot x}\, \mathrm{Tr}\left(e^{-(\mathbf{H}-F)/T}\ T^*\mathbf{J}^\mu(x)\mathbf{J}_\mu(0)\right).$$

From here on we take $T \leq m_\pi$ and consider only pion states. Expanding the trace in terms of incoming pions, and summing over disconnected pieces leads to the virial expansion

$$\begin{aligned}
\mathbf{W}^F(q) = {} & i\int d^4x\, e^{iq\cdot x}\ < 0|\, T^*\mathbf{J}^\mu(x)\mathbf{J}_\mu(0)|0 > \\
& + \sum_a i\int \frac{d^3k}{(2\pi)^3}\frac{n(\omega_k)}{2\omega_k}\int d^4x\, e^{iq\cdot x} \\
& \times < \pi^a(k)\,\mathrm{in}|\, T^*\mathbf{J}^\mu(x)\mathbf{J}_\mu(0)|\pi^a(k)\,\mathrm{in} >_{\mathrm{conn.}} \\
& + \frac{1}{2!}\sum_{a,b}\int \frac{d^3k_1}{(2\pi)^3}\frac{d^3k_2}{(2\pi)^3}\frac{n(\omega_{k_1})}{2\omega_{k_1}}\frac{n(\omega_{k_2})}{2\omega_{k_2}} \\
& \times i\int d^4x\, e^{iq\cdot x} < \pi^a(k_1)\pi^b(k_2)\,\mathrm{in}| \\
& \times T^*\mathbf{J}^\mu(x)\mathbf{J}_\mu(0)|\pi^a(k_1)\pi^b(k_2)\,\mathrm{in} >_{\mathrm{conn.}} \\
& + ... \qquad (5)
\end{aligned}$$

with the pion energy $\omega_k = \sqrt{m_\pi^2 + k^2}$, and the thermal pion distribution $n(\omega) = 1/(e^{\omega/T} - 1)$. The matrix elements in (5) correspond to the forward scattering amplitudes of a virtual photon off on-shell pions, $\gamma^*\, n\pi \to \gamma^*\, n\pi$.

To leading order in the pion density,

$$n = 3\int \frac{d^3k}{(2\pi)^3}\; n(\omega_k),$$

only the first two terms in (5) contribute. A slight refinement is to note that the reduction of one pion is associated with a factor of $1/f_\pi$, where $f_\pi = 93$ MeV is the pion decay constant, so that the dimensionless expansion parameter should be $\kappa = n/2m_\pi f_\pi^2$. According to Ref. [11], a pion gas with a temperature $T \leq m_\pi$ is characterized by a pion mean free path of the order of 2-3 fm over a wide range of momenta, with a pion mean distance of the order of 2 fm. This gives $\kappa = 0.3$, so the truncation should be reasonable.

The absorptive part of the vacuum contribution is directly related to data through e^+e^- annihilation into hadrons [12]. The forward scattering amplitude $\gamma^*\pi \to \gamma^*\pi$ is unfortunately not measurable. However, it can be constrained by data as we now discuss.

3. Decomposing the electromagnetic current into the isovector part $\mathbf{V}^3$ and the isoscalar part $\mathbf{B}$, the forward $\gamma^*\pi \to \gamma^*\pi$ matrix element involves three types of time-ordered correlators **BB**, **BV**, and **VV**. In pionic states, the **BB** and **BV** correlators are expected to be small. Indeed, in the soft pion limit, conventional PCAC gives zero for both matrix elements. The former because **B** commutes with the axial charge, and the latter because the vacuum is isospin invariant. The **VV** correlator in the one-pion state $\mathbf{W}^F$ can be reduced to pertinent vacuum correlators using chiral reduction formulas [9]. The result is ($\nu = k\cdot q$)

$$\begin{aligned}
\mathrm{Im}\,\mathbf{W}^F(q) = {} & -3q^2\mathrm{Im}\,\mathbf{\Pi}_V(q^2) \\
& + \frac{1}{f_\pi^2}\int \frac{d^3k}{(2\pi)^3}\frac{n(\omega_k)}{2\omega_k}\mathbf{W}_1^F(q,k) + \mathcal{O}\left(\kappa^2\right) \qquad (6)
\end{aligned}$$

with

$$\begin{aligned}
& \mathbf{W}_1^F(q,k) = 12q^2\mathrm{Im}\,\mathbf{\Pi}_V(q^2) \\
& - 6(k+q)^2\mathrm{Im}\,\mathbf{\Pi}_A\left((k+q)^2\right) + (q\to -q) \\
& + 8(\nu^2 - m_\pi^2 q^2)\mathrm{Im}\,\mathbf{\Pi}_V(q^2) \\
& \quad \times\mathrm{Re}\left(\Delta_R(k+q) + \Delta_R(k-q)\right) \\
& + 3m_\pi^2 f_\pi \int d^4x d^4y\; e^{iq\cdot(x-y)} \\
& \quad \times\mathrm{Im}\;\langle 0|T^*\mathbf{V}_\mu^3(x)\mathbf{V}^{\mu,3}(y)\hat{\sigma}(0)|0\rangle \\
& - k^\alpha k^\beta \int d^4x d^4y d^4z\; e^{iq\cdot(x-y)}e^{-ik\cdot z} \\
& \quad \times\mathrm{Im}\; i\langle 0|T^*\mathbf{V}_\mu^3(x)\mathbf{V}^{\mu,3}(y)\mathbf{j}_{A\alpha}^a(z)\mathbf{j}_{A\beta}^a(0)|0\rangle \\
& + k^\beta\epsilon^{a3e}\mathrm{Im}\; i\left(\delta_\mu^\alpha - (2k+q)_\mu(k+q)^\alpha\Delta_R(k+q)\right) \\
& \quad \times\int d^4x d^4y\; e^{ik\cdot(y-x)}e^{-iq\cdot x}\langle 0|T^*\mathbf{j}_{A\alpha}^e(x)\mathbf{j}_{A\beta}^a(y)\mathbf{V}^{\mu,3}(0)|0\rangle \\
& + (q\to -q) + (k\to -k) + (q,k\to -q,-k) \qquad (7)
\end{aligned}$$

where $\Delta_R(k)$ is the retarded pion propagator

$$\Delta_R(k) = \mathbf{PP}\frac{1}{k^2 - m_\pi^2} - i\pi\mathrm{sgn}(k^0)\delta(k^2 - m_\pi^2), \qquad (8)$$

$\mathbf{j}_A$ is the axial vector current with the one-pion contribution subtracted, $\mathbf{V}$ is the isovector current discussed above, and $\hat{\sigma}$ is a scalar density related to $\overline{q}q$ [9]. $\mathbf{\Pi}_A$ and $\mathbf{\Pi}_V$ are the transverse part of the axial $< 0|T^*\mathbf{j}_A\mathbf{j}_A|0 >$ and vector $< 0|T^*\mathbf{V}\mathbf{V}|0 >$ correlators respectively. The absorptive part of $\mathbf{\Pi}_V$ follows from electroproduction data, while the absorptive part of $\mathbf{\Pi}_A$ follows from tau decay data.

Note that the longitudinal part of the axial correlator does not contribute here. Taking the chiral limit ($m_\pi = 0$) and for a zero-momentum pion,

$$\mathbf{W}_1^F(q,0) = 12q^2\mathrm{Im}\left(\mathbf{\Pi}_V(q^2) - \mathbf{\Pi}_A(q^2)\right)$$

which reproduces the results obtained in [12,13]. As already indicated, eqs. (6-7) only takes care of the isovector part of the electromagnetic current, both at zero and first order in the virial expansion. The inclusion of the isoscalar contribution to the zeroth order part leaves our arguments unchanged (at the 1% level) except around the phi region.

The third term of (7) contains the principle value integral from (8). However, there is no pole within the range of integration unless $q^2 = 2m_\pi q_0$. This term is proportional to $q^2\mathrm{Im}\mathbf{\Pi}_V(q^2)$ vanishing at $q^2 = 0$.

The last three terms of (7) are vacuum correlators which appear in other low-energy processes and are also constrained by data. The $\mathbf{j}_A\mathbf{j}_A\mathbf{V}$ correlator appears in the radiative decay of the pion [9]. Empirically, the contribution of this term is small at threshold. There are two ways in which this can be checked analytically: a resonance saturation [14] and a one-loop expansion [9]. Both of these methods give zero for this correlator.

The $\mathbf{j}_A\mathbf{j}_A\mathbf{V}\mathbf{V}$ and $\mathbf{V}\mathbf{V}\hat{\sigma}$ correlators appear in the two-photon fusion process [9]. Resonance saturation for both of these gives on the order of a 1% correction and the one-loop result contributes about 1% in the low mass region and even less at higher energies. Both descriptions are in agreement with data from $\gamma\gamma \to \pi^+\pi^-$ [15] and $\gamma\gamma \to \pi^0\pi^0$ [16]. Hence, the last three correlators in (7) may be ignored and the rest can be extracted from data. This information will be used in section 5 to assess the dilepton and photon rate.

The present analysis can be readily carried out to the photon emission rate through

$$q^0 \frac{d\mathbf{R}}{d^3q} = -\frac{\alpha}{4\pi^2}\,\mathbf{W}(q) \tag{9}$$

with $q^2 = 0$. The constraints of current conservation and chiral symmetry apply equally well to the photon emission rate. As indicated above, it is important to assess both emission rates simultaneously for consistency. In our case, the only non-zero contribution comes from the $\mathbf{\Pi}_A$ term in eq. (7).

4. For completeness, we mention another expansion scheme called the Haag expansion. From the pion electromagnetic form factor

$$< \pi^a(p')\pi^b(p)\,\mathrm{in}|\mathbf{S}\mathbf{J}_\mu(x)|0 >=$$
$$= i\epsilon^{a3b}(p'-p)_\mu\; e^{i(p+p')\cdot x}\;\mathbf{F}_V((p+p')^2)$$

and the crossed versions, we obtain the Haag expansion

$$\mathbf{S}\mathbf{J}_\mu(x) = i\epsilon^{a3b}\int \frac{d^3p}{(2\pi)^3}\frac{d^3p'}{(2\pi)^3}\frac{1}{2\omega_p}\frac{1}{2\omega_{p'}}$$
$$\Bigg((p+p')_\mu\,\mathbf{F}_V((p-p')^2)\; a^{a\dagger}_{\mathrm{in}}(p')a^b_{\mathrm{in}}(p)e^{-i(p-p')\cdot x}$$
$$+\frac{1}{2}(p'-p)_\mu\,\mathbf{F}_V((p+p')^2)\; a^{a\dagger}_{\mathrm{in}}(p')a^{b\dagger}_{\mathrm{in}}(p)e^{i(p+p')\cdot x}$$
$$+\frac{1}{2}(p-p')_\mu\,\mathbf{F}_V((p+p')^2)\; a^{a}_{\mathrm{in}}(p')a^{b}_{\mathrm{in}}(p)e^{-i(p+p')\cdot x}\Bigg)$$
$$+\mathcal{O}(\pi^4_{\mathrm{in}})$$

and similarly for $\mathbf{J}_\mu(y)\mathbf{S}^\dagger$, where $\mathbf{S}$ is the hadronic S-matrix. Inserting this into (2), and using energy-momentum conservation along with Wick's theorem, we obtain

$$\mathbf{W}(q) = -\frac{1}{8\pi|\vec{q}|}(q^2-4m_\pi^2)|\mathbf{F}_V(q^2)|^2$$
$$\times\theta(q^2-4m_\pi^2)\int_{\omega_-}^{\omega_+} d\omega\; n(\omega)\,n(q^0-\omega)$$

$$\omega_\pm = \frac{1}{2}q^0 \pm \frac{1}{2}|\vec{q}|(1-\frac{4m_\pi^2}{q^2})^{\frac{1}{2}}. \tag{10}$$

The form factor $\mathbf{F}_V(q^2)$ for $q^2 \geq 4m_\pi^2$ is directly measured from electro-production. For $q^2 < 0$ it follows from pion scattering on hydrogen targets. In both cases, rho dominance holds to a good accuracy. This is similar to the first term in the virial expansion (5), but the Haag expansion is presumably less controlled. In particular, the photon rate is zero in this approximation. We note that (10) in the $\vec{q} = 0$ limit has already been used in [4].

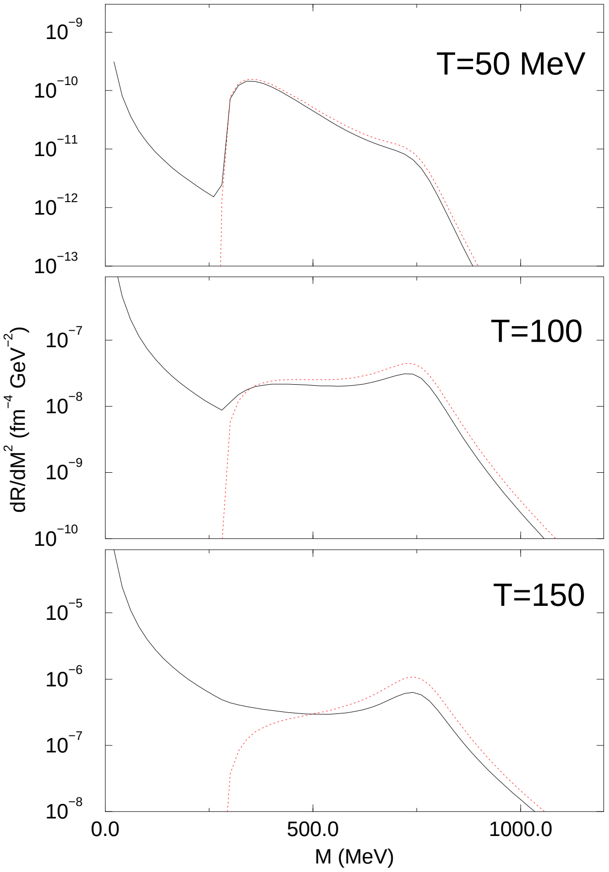

FIG. 1. The total integrated rate for dielectrons from a hadronic gas of $T = 50, 100$ and 150 MeV. The solid line is from the virial expansion and the dotted line from the Haag expansion.

5. In Fig. 1, we show the numerical results following from the above analysis for the dielectron rate as a function of the invariant dielectron mass $M = \sqrt{q^2}$, all the way up to the $a1$ mass for the temperatures T = 50, 100, 150 MeV. The change of variables to the rapidity y and magnitude of the transverse momentum $q_\perp$ [10]

$$\frac{d\mathbf{R}}{d^4q} = \frac{2}{\pi}\frac{d\mathbf{R}}{dM^2\,dy\,dq_\perp^2}$$

and an integration over y and $q_\perp^2$ is performed. The solid curve is the result following from (1) using (4) and (6). The dotted curve is the result following from (1) and the Haag expansion (10). For comparison, we also show the integrated dimuon rate in Fig. 2. As the temperature increases the rate for dilepton momentum below the rho pole increases with respect to the Haag expansion. The rate is always cut off at the dilepton threshold by phase space (3).

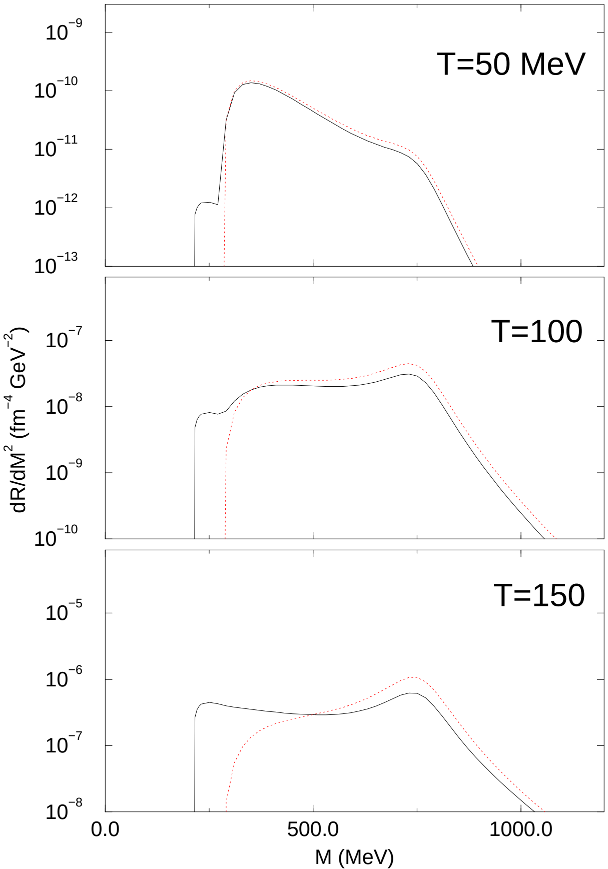

FIG. 2. The total integrated rate for dimuons from a hadronic gas of $T = 50, 100$ and 150 MeV. The solid line is from the virial expansion and the dotted line from the Haag expansion.

For a parameterization of $\mathbf{F}_V$, we used the common Breit-Wigner form with a varying width as found in [17] and a small correction for large q^2 to fit the data [18].

$$\mathbf{F}_V(q^2) = \frac{m_\rho^2 + \gamma q^2}{m_\rho^2 - q^2 - i m_\rho \Gamma_\rho(q^2)} \tag{11}$$

with a non-zero width only for $q^2 > 4m_\pi^2$ [17]

$$\Gamma_\rho(q^2) = 0.149 \frac{m_\rho}{\sqrt{q^2}} \left(\frac{q^2 - 4m_\pi^2}{m_\rho^2 - 4m_\pi^2} \right)^{3/2} \text{GeV} \tag{12}$$

and $\gamma = 0.4$.

For the terms in (6) depending on Im $\mathbf{\Pi}_V$, our results will be sensitive to the momentum dependence of the width. The KSFR relation implies [9]

$$\mathbf{F}_V(q^2) = 1 + \frac{q^2}{2f_\pi^2}\mathbf{\Pi}_V(q^2) + \mathcal{O}\left(\frac{1}{f_\pi^4}\right),$$

so we have fixed $\mathbf{\Pi}_V$ from $\mathbf{F}_V$ with the $1/f_\pi^4$ terms omitted. Fig. 3 shows this fit against the data taken from the recent compilation by Huang [12]. Using the fit instead of the data produces a 10% uncertainty at the rho pole where the fit is worst. On the log plot of Fig. 1 this is a negligible difference.

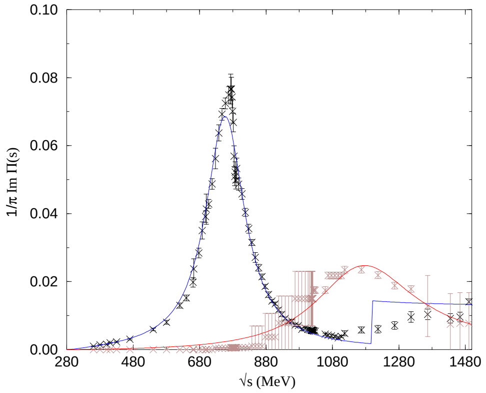

FIG. 3. Data for the vector and axial spectral densities and the fits we used.

The axial channel is dominated by the $a1(1260)$. A Breit-Wigner fit for $\mathbf{\Pi}_A$ works well with $(f_A, m_A) = (190, 1210)$ MeV through the substitution $m_\rho^2 + \gamma q^2 \to f_A^2$, $m_\rho \to m_A$, and $\Gamma_\rho(q^2) \to \Gamma_A(q^2)$ in (11). In (12), the threshold is moved to $9m_\pi^2$ with $(m_\rho, 4m_\pi^2) \to (m_A, 9m_\pi^2)$ and the overall constant is changed so that $\Gamma_A(m_A^2) = 0.4$ GeV. The comparison of this fit to the data is also shown in Fig. 3. We note that fixed-width calculations tend to overestimate the tail of the $a1$ in the low mass region by a large factor.

In Fig. 4, we show the non-integrated results for back-to-back ($\vec{q} = 0$) dielectrons with $T = 50, 100, 150$ MeV. As in the fully integrated rate, our result and the Haag expansion are practically identical for the lower temperatures and, as the temperature increases, the region below the two pion threshold increases with respect to the Haag rate.

The shape of the virial expansion curves in Figs 1, 2, and 4 can be explained as follows. Above the two-pion threshold, the first term of eq. (6) dominates giving the rho peak. As the temperature increases, the Im $\mathbf{\Pi}_V$ terms in eq. (7) start to play a part and, since they give a negative contribution to the rate, decrease the rho peak by about 10% for $T = 150$ MeV. The Im $\mathbf{\Pi}_V$ terms are proportional to $\Gamma_\rho(q^2)$ and as a consequence all vanish below the two-pion threshold. This part is fully consistent with the Haag rate for all temperatures.

The main difference comes from the inclusion of the Im $\mathbf{\Pi}_A$ term. It is the only contribution below the two-pion threshold. The reason it picks up the $a1$ pole contribution even at low q^2 is because, in contrast to the result in the chiral limit, the axial spectral density is integrated over all momentum in the thermal averaging. This weakens the contribution from the $(k+q)^2$ prefactor in eq. (7) therefore allowing the $1/q^2$ dependence in (1) to dominate at low q^2. Integrating the rate pronounces this even more and is only cut off at the dilepton threshold by (3).

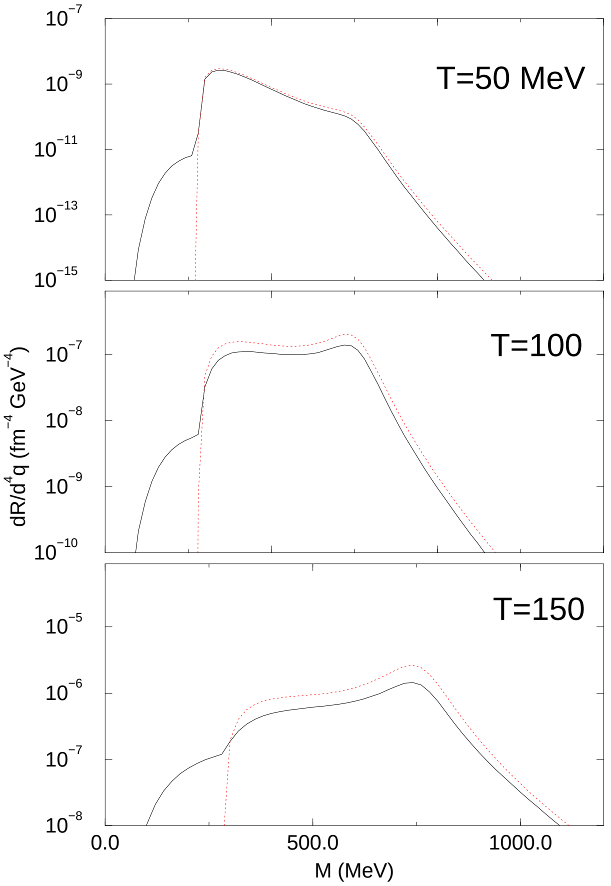

FIG. 4. The back-to-back rate for dielectrons. The virial expansion is the solid line and the Haag expansion is the dotted line.

This enhancement can be physically understood as follows. Since $2\,\mathrm{Im}\,\mathbf{W}^F(q) = \mathbf{W}(q) + \mathbf{W}(-q)$, the low-mass region is enhanced by processes such as $\mathbf{X} \to \pi e^+ e^-$ through $\mathbf{W}(-q)$. These are reminiscent of the Dalitz decays. This description, however, is very qualitative since the relationship between the physical reactions in the emission rate and the imaginary part gets blurred by the virial expansion. In comparison with most dilepton rate calculations [4,12,19,20], our results show a substantial enhancement in the low mass dilepton region (2-4 m_π), for $T = 100$-150 MeV.

For dileptons of mass above the $a1$ pole, our emission rate is also larger than the one expected from the Haag expansion due to the contribution from the continuum in the rho channel as well as the effects from the $a1$. At $T = 150$ MeV the enhancement is about an order of magnitude in the dielectron rate.

If we were to assume an acceptance factor of about 1/100 (corresponding to the experimental cuts in $q_\perp$ and y), a lifetime for the thermal gas of 5 fm/c, and a normalization of $2n$ (due to charged particle multiplicities), our dielectron rate distribution at a temperature of 100-150 MeV is similar in shape and magnitude to the physically measured dielectron rate by the CERES collaboration [1]. In addition, our dimuon rate distribution for a temperature of 50-100 MeV is similar in shape to those measured by the HELIOS3 collaboration [2] prior to the experimental acceptance cuts. Of course, these are purely heuristic statements that should motivate a more detailed calculation using a transport equation.

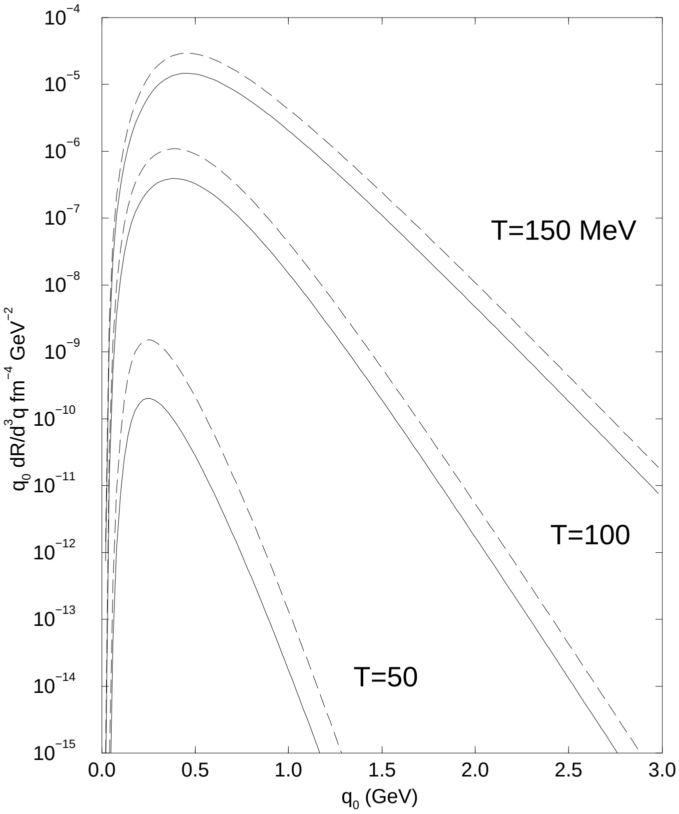

FIG. 5. The photon emission rate from a hot hadronic gas. The solid and dotted lines were calculated with a pion chemical potential of 0 and 100 MeV respectively.

Fig. 5 shows the photon emission rate versus the photon energy for $T = 50, 100, 150$ MeV. The solid line is the result following from the virial expansion. As we have noted, there is no contribution from the Haag expansion to the order quoted. We note that the the bulk of the low mass dileptons stem primarily from the photon source. Our results are an order of magnitude above those obtained using two-body reactions with thermal ρ's and $a1$'s [20,21] at the peak of the curve. However, above the $a1$ mass, our results are in agreement with others. We note that the use of a constant width for Γ_A increases the rate by almost an order of magnitude for all temperatures.

Other calculations [21] tend to underestimate the pion electric polarizability by almost an order of magnitude which could point to the source of their result being smaller. In our case, the result is constrained by the data for $\mathbf{\Pi}_A$.

The role of the pion chemical potential μ_π may be assessed through the substitution $n(\omega) = (e^{\omega/T} - 1)^{-1} \rightarrow (e^{(\omega-\mu_\pi)/T} - 1)^{-1}$ in the above formulas. A non-zero chemical potential influences all terms which involve pions. This includes the entire Haag rate. In contrast, the first term in the virial expansion, which is its dominant contribution around the rho pole, is not influenced.

Fig 6. shows the rates for $\mu_\pi = 100$ MeV which describes a dilute system of pions with a mean pion separation of about 2 fm at T = 100-150 MeV [11]. The dilepton integrated rate following from the virial expansion is enhanced in the low mass region by about a factor of five. There is no change near the rho pole and above 1 GeV it is again slightly enhanced. The entire Haag rate, on the other hand, is increased by about a factor of 10. This is a major qualitative difference in the two analyses. This further enhancement points at the importance of pions off-equilibrium, thereby motivating a more quantitative analysis in the context of kinetic theory. The photon rates are systematically enhanced as shown by the dotted lines in Fig. 5. In the temperature range T = 100-150 MeV, the enhancement is about a factor of two throughout the photon energy spectrum.

6. To summarize, we have argued that for a hadronic gas at temperatures $T \leq m_\pi$ the dilepton and photon emission rates were constrained by data from electroproduction, tau decays, radiative pion decay and two-photon fusion reactions. Through these constraints, the rates were assessed using data for the various vacuum correlation functions and carried out to the first two terms in the virial expansion (5). For completeness, we have compared the results following from the Haag expansion.

Through chiral reduction formulas, our construction shows the interdependence between the dilepton and photon rates and other low energy processes. We note that the chiral reduction formulas follow solely from broken chiral symmetry with explicit (2,2) breaking. They are a direct generalization of current algebra results from threshold to general momenta. In this respect, our analysis is different from finite temperature arguments using PCAC in the chiral limit [12,13]. Our analysis was confined to the isovector part of the electromagnetic current, and could be improved at higher mass (phi region) by including the isoscalar contribution.

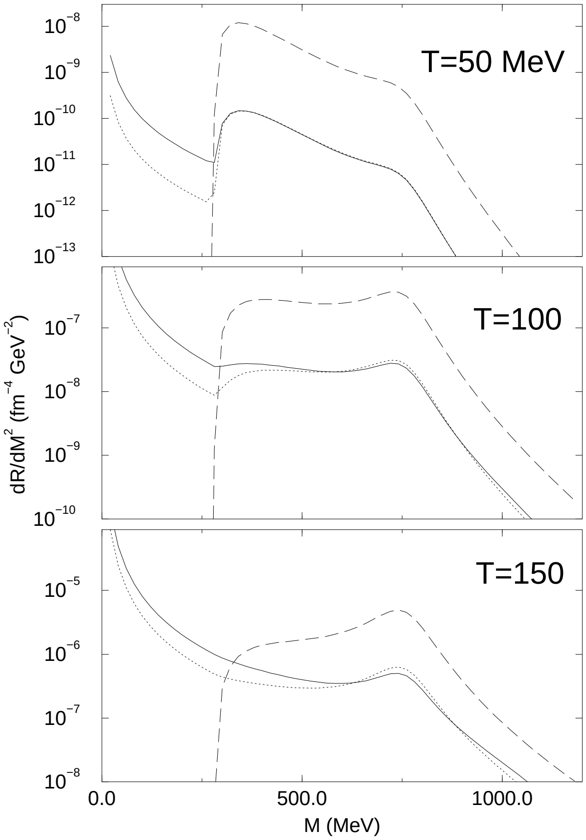

FIG. 6. The dielectron integrated rates for $T = 50, 100, 150$ MeV and a finite pion chemical potential $\mu_\pi = 100$ MeV. The solid line is from the virial expansion. The dashed line is from the Haag expansion. For comparison, the virial expansion result at zero chemical potential is shown as the dotted line.

Since dilepton or photon emission from heavy-ion collisions involve a dynamical integration over the real-time history of the hadronic gas that is expected to expand and cool, our results are only suggestive. However, they already show a thermal pion gas in equilibrium yields dilepton and photon rates that are enhanced in the low mass region compared to most of the calculations using specific reaction processes. The inclusion of a pion chemical potential enhances the entire photon rate and the low and high mass dilepton rates without affecting the rate distribution around the rho mass. These results are relevant for present dilepton measurements at CERES and HELIOS3 as well as future dilepton and photon measurements at RHIC and LHC.

Acknowledgements

We would like to thank Gerry Brown, Robert Pisarski, Madappa Prakash and Heinz Sorge for discussions. We are grateful to Zheng Huang for providing us with his newly compiled data. This work was supported in part by the US DOE grant DE-FG-88ER40388.

---

[1] G. Agakichiev, *et al.*, Phys. Rev. Lett. 75 (1995) 1272.

[2] M. Masera for the HELIOS-3 Collaboration, Nucl. Phys. A 590 (1995) 93c.

[3] R. Santo, *et al.*, Nucl. Phys. A 566 (1994) 61c; R. Albrecht, *et al.*, Nucl. Phys. A 590 (1995) 81c.

[4] C. Gale and J. Kapusta, Nucl. Phys. B 357 (1991) 65.

[5] C. Gale and P. Lichard, Phys. Rep. D 49 (1994) 3338.

[6] E.V. Shuryak Phys. Lett. B 79 (1978) 135; K. Kajantie and H.I. Miettenen, Z. Phys. C 9 (1981) 341; K. Kajantie, J. Kapusta, L. McLerran, and A. Mekjian, Phys. Rev. D 34 (1986) 2476; E. Braaten, R.D. Pisarski, and T.C. Yuan, Phys. Rev. Lett. 64 (1990) 2242; H.A. Weldon, Phys. Rev. Lett. 66 (1991) 293; D. Srivastava and B. Sinha, Phys. Rev. Lett. 73 (1994) 2421.

[7] G.Q. Li, C.M. Ko, and G.E. Brown, to be published.

[8] R.D. Pisarski, hep-ph/9503330 and references therein.

[9] H. Yamagishi and I. Zahed, Ann. Phys. to be published, hep-ph/9503413; H. Yamagishi and I. Zahed, Phys. Rev. D 53 (1996) 2288.

[10] L.D. McLerran and T. Toimela, Phys. Rev. D 31 (1985) 545.

[11] J.L. Goity and H. Leutwyler, Phys. Lett. B 228 (1989) 517; M. Prakash, M. Prakash, R. Venugopalan, and G. Welke, Phys. Rep. 227 (1993) 321.

[12] Z. Huang, Phys. Lett. B 361 (1995) 131.

[13] M. Dey, V.L. Eletsky, and B.L. Ioffe, Phys. Lett. B 252 (1990) 620; V.L. Eletsky, Phys. Lett. B 245 (1990) 229; V.L. Eletsky and B.L. Ioffe, Phys. Rev. D 51 (1995) 2371.

[14] S. Chernyshev and I. Zahed, hep-ph/9511271.

[15] J. Boyer, *et al.*, Phys. Rev. D 42 (1990) 1350.

[16] H. Marsiske, *et al.*, Phys. Rev. D 41 (1990) 3324.

[17] G.E. Brown, M. Rho, and W. Weise, Nucl. Phys. A454 (1986) 669.

[18] J.V. Steele, H. Yamagishi, and I. Zahed, submitted to Ann. Phys, hep-ph/9505330.

[19] C. Song, S.H. Lee, and C.M. Ko, Phys. Rev. C 52 (1995) 476; C. Song, C.M. Ko, and C. Gale, Phys. Rev. D 50 (1994) 1827.

[20] J.K. Kim, P. Ko, K.Y. Lee, and S. Rudaz, hep-ph/9602293.

[21] J. Kapusta, P. Lichard, and D. Seibert, Phys. Rev. D 44 (1991) 2774; L. Xiong, E.V. Shuryak, and G.E. Brown, Phys. Rev. D 46 (1992) 3798; C. Song, Phys. Rev. C 47 (1993) 2861.